Analytic modelling of passive microfluidic mixers

Alexi Bonament, Alexis Prel, Jean-Michel Sallese, Christophe Lallement, Morgan Madec

▶ **To cite this version:**

Alexi Bonament, Alexis Prel, Jean-Michel Sallese, Christophe Lallement, Morgan Madec. Analytic modelling of passive microfluidic mixers. Mathematical Biosciences and Engineering, 2022, 19 (4), pp.3892-3908. 10.3934/mbe.2022179 . hal-03981671

HAL Id: hal-03981671
https://hal.science/hal-03981671

Submitted on 9 Feb 2023

HAL is a multi-disciplinary open access archive for the deposit and dissemination of scientific research documents, whether they are published or not. The documents may come from teaching and research institutions in France or abroad, or from public or private research centers.

L'archive ouverte pluridisciplinaire **HAL**, est destinée au dépôt et à la diffusion de documents scientifiques de niveau recherche, publiés ou non, émanant des établissements d'enseignement et de recherche français ou étrangers, des laboratoires publics ou privés.

Mathematical Biosciences and Engineering

MBE, 19 (4): 3892–3908.
DOI: 10.3934/mbe.2022179
Received: 14 October 2021
Revised: 04 January 2022
Accepted: 24 January 2022
Published: 11 February 2022

http://www.aimspress.com/journal/MBE

Research article

Analytic modelling of passive microfluidic mixers

Alexi Bonament[1], Alexis Prel[1], Jean-Michel Sallese[2], Christophe Lallement[1] and Morgan Madec[1]

[1] Laboratory of Engineer Sciences, Computer Science and Imagine (ICube), UMR 7357 (Université de Strasbourg/Centre National de Recherche Scientifique), Strasbourg, France
[2] STI-IEL-Electronics Laboratory, Ecole Polytechnique Fédérale de Lausanne (EPFL), Lausanne, Switzerland

* **Correspondence:** Email: morgan.madec@unistra.fr; Tel: +336-86-77-98-23.

Abstract: This paper deals with a new analytical model for microfluidic passive mixers. Two common approaches already exist for such a purpose. On the one hand, the resolution of the advection-diffusion-reaction equation (ADRE) is the first one and the closest to physics. However, ADRE is a partial differential equation that requires finite element simulations. On the other hand, analytical models based on the analogy between microfluidics and electronics have already been established. However, they rely on the assumption of homogeneous fluids, which means that the mixer is supposed to be long enough to obtain a perfect mixture at the output. In this paper, we derive an analytical model from the ADRE under several assumptions. Then we integrate these equations within the electronic-equivalent models. The resulting models computed the relationship between pressure and flow rate in the microfluidic circuit but also takes the concentration gradients that can appear in the direction perpendicular to the channel into account. The model is compared with the finite element simulation performed with COMSOL Multiphysics in several study cases. We estimate that the global error introduced by our model compared to the finite element simulation is less than 5% in every use case. In counterparts, the cost in terms of computational resources is drastically reduced. The analytical model can be implemented in a large range of modelling and simulation languages, including SPICE and hardware description language such as Verilog-AMS. This feature is very interesting in the context of the *in silico* prototyping of large-scale microfluidic devices or multi-physics devices involving microfluidic circuits, *e.g.* lab-on-chips.

Keywords: microfluidics; passive mixer; modelling; analytic models; hardware description languages; COMSOL simulations; electronic-equivalent microfluidic circuits; Verilog-AMS

1. Introduction

The development of microfluidics has been booming in recent years, with many applications in the pharmaceutics [1], biology [2], healthcare [3] or environmental monitoring [4]. However, the design and the manufacturing of microfluidic circuits still require a large deal of expertise both on engineering and on technological aspects. Today, most of the microfluidic designs are still performed with long and costly trial-and-error processes. One possible promoter for the democratization of microfluidics could be the development of technological standards allowing realization of microfluidic circuits on demand, and thus its design by engineers *in silico* without deep knowledge of the whole technological process. Following the path of electronics in the 90s, this transition requires dedicated computer-aided design tools and associated mathematical models in adequacy with the standard technologies. Many investigations have already been done for years in this avenue: numerical simulation of continuous microfluidic devices [5,6], droplets formation [7], particle flow [8], electroosmotic flows [9] or fluid active and passive mixing [10,11]. Moreover, microfluidics is rarely isolated in a system but interacts with other domains such as chemistry or biochemistry, electronic sensors, light or thermal phenomena, etc. All the models associated with all of these different parts of a lab-on-a-chip must therefore be interoperable and thus, implementable in the same computational environment.

In this paper, the focus is put on continuous microfluidics and more specifically on passive mixers [10]. Continuous microfluidics concerns all applications where flows are laminar, *i.e.* flow for which viscous forces are dominant. The Reynolds number is a dimensionless parameter usually used to determine if these conditions are met [12]. A passive mixer is, as its name indicates, a microfluidic circuit allowing the mixing of two fluids under continuous microfluidic conditions. Most passive mixers are Y-shaped junction, as depicted in Figure 1. Because of the predominance of viscosity forces, mixing fluids in laminar conditions is not trivial. The mixture is only due to passive diffusion of molecules in the transverse direction along the channel [13,14], which is only effective after a given length of the channel. This parameter is called the mixing length and corresponds approximately to the ratio between the flow rate of the fluid and the diffusion coefficient of the chemical species involved.

Generally speaking, the simulation of microfluidic circuits can be performed in two ways. On the one hand, fluid behavior and molecular diffusion inside microfluidic channels are respectively governed by the Navier-Stokes equations [15] and the reaction-advection-diffusion equation [16]. Both of them are partial differential equations (PDE) that must be solved by finite element simulators[17]. Commercial simulators (*e.g.* COMSOL Multiphysics [18] and more specifically its Microfluidic Module [19]), or academic open-source simulators (*e.g.* FeelPP [20]) natively implemented such features. This approach provides very accurate and faithful results towards actual behavior of the fluids. The downside is the heaviness of models from a computational perspective. Consequently, such tools are very suitable for design and the study of a microfluidic device alone, but can quickly become limiting for the simulation of this device as a part of a complete microfluidic system.

On the other hand, analytical models can be used to describe the behavior of microfluidic devices in a simplified but accurate way. By opposition to physical models, analytic models are only composed of time-derivative terms. A common approach used to write analytic models of microfluidic circuits is the analogy that has been demonstrated for years between electrical circuits and microfluidic circuits [21,22]. According to this analogy, flows are considered as electric currents, pressure differences as potential differences and channels as hydraulic resistance in the sense that a pressure difference at the two ends of a channel produces a flow which intensity depends on the channel

geometry. Thus, a microfluidic system can be analyzed according to its derived electronic-equivalent circuits. Such method has already been applied to the simulation and the *in silico* design of passive mixers [23,24]. Although very suitable to predict the relationship between pressure and flow at the inlets and the outlets of the device, electronic-equivalent models lack of accuracy in the description of the mixture itself. In particular, they are based on the homogeneous fluid assumption or, which is another way to put it, are only valid for channels which lengths are long enough compared to the fluid diffusion length.

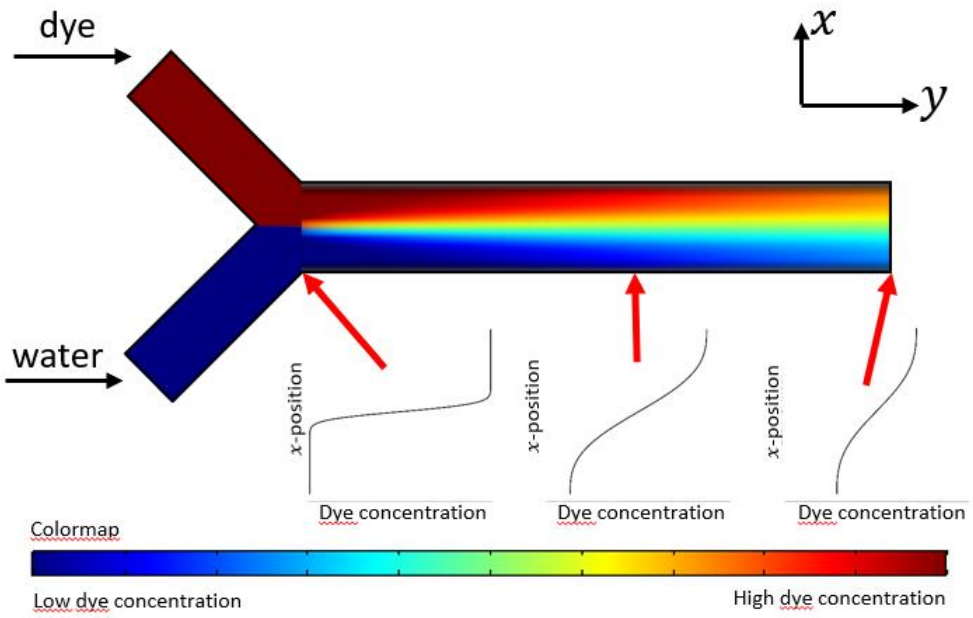

Figure 1. Schematic of the Y-shaped passive mixer. The device is composed of two inlets (here, one is the water and the other is a dye) and one outlet. As we can see on this cartoon (which is purely illustrative and not a simulation result), the mixing is established along the channel and, for a short channel, the dye concentration is not homogeneous in the x direction.

This paper deals with the opportunity to enrich electronic equivalent modelling approach by adding an analytical model for the transverse concentration profile within the channel. The theoretical background, our assumptions and the way the model is implemented are described in the "Material and Method" section. The "Result" includes all the results of simulations performed to compare the analytic model with COMSOL. Finally, the validity of this approach and its interest in the context of *in silico* prototyping of large-scale microfluidic devices is discussed in the last part of the paper.

2. Materials and methods

2.1. Theoretical background

2.1.1. Poiseuille's flow

First, let us consider a long cylindrical channel of radius R. Let the y-axis be the direction along

the channel. At steady state, the velocity field $\mathbf{u}$ is unidirectional and laminar. Due to the boundary condition (*i.e.* $\mathbf{u} = 0$ at $r = R$), the pressure-driven fluid velocity inside the channel has a parabolic profile. The y-component u_y of $\mathbf{u}$ can be modelled as a function of the radial distance r by the following equation, called Poiseuille's flow:

$$u_y(r) = u_{max} \cdot \left(1 - \frac{r^2}{R^2}\right) \tag{1}$$

where u_{max} (in $\mathrm{m} \cdot \mathrm{s}^{-1}$) is the maximum velocity at the centre of the channel. This quantity is proportional to the ratio of the flow rate Q (in $\mathrm{m}^3 \cdot \mathrm{s}^{-1}$) and the channel section S (in m^2).

2.1.2. Advection-diffusion-advection-reaction law

The structure of a passive mixer is depicted in Figure 1. It is composed of a Y-shaped junction at which two homogeneous laminar flow join together and a straight channel in which both fluids mix together. However, in this channel, flows are still laminar and the mixing is only due to the passive diffusion in the transverse direction.

Generally speaking, the concentration of a given molecule inside a microfluidic device is described by the advection-diffusion-reaction equation (ADRE) [15]. All along this paper, we reduce the study down to a two-dimensional problem, assuming the system invariant by translation along the z-axis. The 2D-ADRE equation is the following:

$$\frac{\partial C}{\partial t} = D \cdot \Delta C - \mathbf{u}(x, y, t) \circ \nabla C + s(x, y, t) \tag{2}$$

where C is the concentration of a given molecule (in $\mathrm{mol} \cdot \mathrm{L}^{-1}$), D is the diffusion coefficient of that molecule (in $\mathrm{m}^2 \cdot \mathrm{s}^{-1}$), $\mathbf{u}(x, y, t)$ is the velocity field of the fluid (in $m \cdot \mathrm{s}^{-1}$), $s(x, y, t)$ is a local source (or a sink, depending on its sign) of molecule which can be due, for instance, to chemical reactions occurring in the channel, Δ is the Laplacian operator, ∇ is the gradient operator and $\circ$ is the dot product.

2.2. Analytical solution for the 2D-ADRE

2.2.1. Assumptions and validity domain

In a straight channel, due to the laminar flow, transverse component of the fluid velocity can be neglected. Moreover, we consider the microfluidic system at its stationary state. The field velocity does not depend on the time nor on the position along the channel axis. Thus, the velocity field has only one component along y-axis and depends only on x (*i.e.* $\mathbf{u}(x, y, t) = u_y(x) \cdot \mathbf{y}$). Finally, we assume that no chemical reaction occurs inside the channel (*i.e.* $s(x, y, t) = 0$). The ADRE can thus be simplified as following:

$$\frac{\partial C}{\partial t} = D \cdot \left(\frac{\partial^2 C}{\partial x^2} + \frac{\partial^2 C}{\partial y^2}\right) - u_y(x) \cdot \frac{\partial C}{\partial \mathrm{y}} \tag{3}$$

The last assumption concerns the displacement of molecules along the channel direction. The

displacement due to the passive diffusion is assumed to be negligible in comparison to the displacement due to the advection. This point is validated *a posteriori* by COMSOL simulations. We showed that simulation results performed with an isotropic diffusion constant and anisotropic diffusion vector ($D_x = D$ and $D_y = 0$) are quite similar within a large range of flow rate. Under this assumption, equation (3) now becomes:

$$\frac{\partial C}{\partial t} = D \cdot \frac{\partial^2 C}{\partial x^2} - u_y(x) \cdot \frac{\partial C}{\partial y} \tag{4}$$

At the steady state, equation (4) can be rewritten as following:

$$D \cdot \frac{\partial^2 C}{\partial x^2} - u_y(x) \cdot \frac{\partial C}{\partial y} = 0 \tag{5}$$

2.2.2. Reference frame change

To further simplify equation (5), we switch from the Earth reference frame to a new reference frame centred on a point that follows the diffusion front, *i.e.* a reference frame moving at a velocity $u_y(x)$ along the y-axis. Let (x', y') be the coordinate system in this new reference frame. The transition equations between both coordinate systems are the following:

$$\begin{aligned} x' &= x \\ y' &= y - u_y(x) \cdot t \end{aligned} \tag{6}$$

In this new reference frame, equation (5) becomes:

$$\mathrm{D} \cdot \frac{\partial^2 C}{\partial x'^2} - u_y(x) \cdot \frac{\partial C}{\partial t} \cdot \frac{\partial t}{\partial y'} \cdot \frac{\partial y'}{\partial y} = 0 \tag{7}$$

According to equation (6), $\partial y'/\partial y = 1$ and $\partial y'/\partial t = -u_y(x)$. Equation (7) can be simplified as following:

$$\frac{\partial C}{\partial t} = -D \cdot \frac{\partial^2 C}{\partial x'^2} \tag{8}$$

For the sake of simplicity, single quotation marks have been dropped in the following.

2.2.3. Variable separation

We solve equation (8) with the variables separation method which consists of assuming that the function $C(x,t)$ is the product of a function depending only on the time $C_T(t)$ and a function depending only on the position on the *x*-axis $C_X(x)$.

$$C(x,t) = C_X(x) \cdot C_T(t) \tag{9}$$

Using this expression of $C(x,t)$ in equation (8) gives

$$\frac{\mathrm{d}C_T}{\partial t} \cdot C_X = -D \cdot C_T \cdot \frac{\mathrm{d}^2 C_X}{\partial x^2} \tag{10}$$

Separating C_T and C_X terms on both sides of the equality leads to:

$$\frac{1}{D \cdot C_T}\frac{\mathrm{d}C_T}{\partial t} = -\frac{1}{C_X} \cdot \frac{\mathrm{d}^2 C_X}{\partial x^2} \tag{11}$$

This equation has to be true whatever the values of x and t. As a consequence, the only valid solution is to have both terms of equation (11) equal to a constant. Let α be this constant.

2.2.4. Time-dependent solution

Let us first consider the time-dependent term. The left term of equation (11) is a first-order ordinary differential equation (ODE) with a constant second term. Such equation converges only for negative values of α. To avoid any ambiguity about the sign of α, we introduce a new constant λ in such a way that $\alpha = -\lambda^2$. The solution of the first-order ODE is

$$C_T(t) = C_T(0) \cdot e^{-\lambda^2 \cdot D \cdot t} \tag{12}$$

2.2.5. Space-dependent solution

Let us now consider the space-dependent term. The right term of equation (11) is a second-order ODE with a constant negative second term. The solution is supposed to be a combination of sine waves. However, we know from observations and/or finite element simulations that the concentration profile is sigmoidal in the channel [13]. We therefore look for the solution as Fourier series decomposition of $C_X(x)$ Matching with equation (11). For that purpose, let first introduce $\widehat{C_X}(x)$, an extension of $C_X(x)$ on $\mathbb{R}$ (*i.e.* beyond the boundaries of the channel) which is periodic with a period of $2 \cdot W$ where W is the channel width. The expression of $\widehat{C_X}(x)$ as a Fourier series decomposition is the following

$$\widehat{C_X}(x) = \sum_{n=0}^{\infty} A_n \cdot \sin(\lambda_n \cdot x) + B_n \cdot \cos(\lambda_n \cdot x) \tag{13}$$

where n is the order of the Fourier term, A_n and B_n are the Fourier coefficients and λ_n is the value of λ associated with the n-th term of the series. Because of boundaries conditions, i.e. $d\widehat{C_X}/dx = 0$ for $x = 0$ and $x = W$, $A_n = 0 \; \forall \; n$ and :

$$\lambda_n = \frac{n \cdot \pi}{W} \tag{14}$$

2.2.6. Full solution

Putting equations (12) and (14) together leads to the final expression for $C(x,t)$:

$$C(x,t) = \sum_{n=0}^{\infty} B_n \cdot \cos\left(\frac{n \cdot \pi \cdot x}{W}\right) \cdot \mathrm{e}^{-D \cdot t \cdot \left(\frac{n \cdot \pi}{W}\right)^2} \tag{15}$$

with B_n computed from the concentration profile at the start of the channel $C_0(x)$:

$$B_n = \frac{1}{W} \cdot \int_{-W}^{W} C_0(x) \cdot \cos\left(\pi \cdot n \cdot \frac{x}{W}\right) \cdot dx \tag{16}$$

Finally, using the reference frame change backwards, we can establish that $y = y' + u_y(x) \cdot t$. As the reference frame follows the diffusion front, $y' = 0$ and thus $y = u_y(x) \cdot t$. Replacing t by y in equation (15) gives the concentration map as a function of x and y in the channel:

$$C(x, y) = \sum_{n=0}^{\infty} B_n \cdot \cos\left(\frac{n \cdot \pi \cdot x}{W}\right) \cdot \mathrm{e}^{-\frac{D}{u_y} y \cdot \left(\frac{n \cdot \pi}{W}\right)^2} \tag{17}$$

2.3. Concentration profile at the beginning of the channel

According to equations (16) and (17), the concentration profile throughout the channel depends on the initial concentration profile $C_0(x)$. Establishing an analytical expression based on theoretical considerations for $C_0(x)$ is very tricky. However, we know that $C_0(x)$ always exhibits a sigmoidal profile. It can be thus approximated by an empirical model:

$$C_0(x) = \frac{a}{1 + \mathrm{e}^{-b \cdot (x - c)}} + d \tag{18}$$

with a, b, c and d four fitting parameters. The literature and simulations we performed with COMSOL Multiphysics gave us empirical equation to predict the values of these four parameters. a is the amplitude of the sigmoid which depends on the difference of concentration for the molecule of interest in both inlets ($a = C_2 - C_1$). d is the reference concentration level, *i.e.* the concentration level at the inlet 1 ($d = C_1$). c is the position of the inflection point on the x-axis. This value depends mostly on the ratio of the flow rate at both inlets ($c = W \cdot Q_1/(Q_1 + Q_2)$). It should be mentioned that this estimation of c is very coarse at the beginning of the channel because of perturbations due to the mixing but becomes reliable after a few tenths of micrometres. Finally, b represents the steepness of the sigmoid at the inflection point. b is hard to estimate a priori but we establish with a large set of COMSOL simulations that there is a linear relationship between b and the total flow rare ($b = k_1 \cdot (Q_1 + Q_2) + k_2$). The two empirical parameters k_1 and k_2 only depends on the geometry of the Y-shaped junction and have to be extracted from COMSOL simulations once per junction geometry.

2.4. Extraction procedure for sigmoid parameters

Depending on the application, it can be useful to estimate a, b, c and d either from the flow/concentration on mixer inlets or from an arbitrary profile $C(x)$. This can obviously be performed using commonplace optimization methods but also following a specific extraction procedure described in this subsection. For the sake of simplicity, let us rewrite the sigmoid as following:

$$C(x) = \frac{2 \cdot (a' - d')}{1 + \mathrm{e}^{b \cdot (x - c)}} + d' \tag{19}$$

Now (c, a') is the coordinate of the inflection point of $C(x)$, $2 \cdot d'$ is the amplitude of the sigmoid and b is still related to the steepness of the curve at the inflection point.

2.4.1. Computation of a' and c

The inflection point of $C(x)$ corresponds to the maxima of the derivative $C'(x)$. The first step of the extraction procedure is therefore the numerical calculation of this derivative. Then, the apex of the derivative is accurately calculated using a second-degree interpolation polynomial $L(x) = \alpha \cdot x^2 + \beta \cdot x + \gamma$. The coefficients α, β and γ of this polynomial corresponds to the Lagrange interpolation with the three highest points of $C'(x)$ and thus can be computed analytically from the coordinates of these points. The computation of c from $L(x)$ is straightforward: $c = \beta/2 \cdot \alpha$. Finally, $a' = C(c)$ is computed from a linear interpolation of $C(x)$ with two points surrounding $x = c$.

2.4.2. Computation of b and d'

The slope s at the inflection point can be calculated in two ways: i) from the interpolation polynomial: $s = L(c) = \alpha \cdot c^2 + \beta \cdot c + \gamma$ or ii) from the derivative of the sigmoidal function $s = C'(c) = b \cdot (d' - a')/2$. This gives a relationship between b and a', c and d':

$$b = \frac{2 \cdot (\alpha \cdot c^2 + \beta \cdot c + \gamma)}{d' - a'} \tag{20}$$

The parameter d' is the amplitude of the sigmoid which can be easily computed from the curve if and only if we can consider that $C(x)$ reach its asymptotes at $x = 0$ and $x = W$. But this is, however, not necessarily the case. Thus, a simple iterative method is implemented, starting with $d' = C((W) - C(0))/2$ and increasing d' step-by-step up to value that minimise the root mean square error (RMSE) between the sigmoid obtained with fitted parameters and the actual values of $C(x)$.

3. Results

In this part, the validation procedure for our analytical model is described. In principle, the validation of a model goes by a comparison with experimental results. However, as the passive mixer is a very simple microfluidic circuits, we can trust COMSOL simulations to faithfully reproduce reality: COMSOL's performance for simulating microfluidic mixers in laminar flow has already been proved even for circuits more sophisticated than those studied in this paper *e.g.* mixers including semicircle elements [25] and trapezoidal blades [26]. Therefore, we opted in this study for a validation of our model by comparison with COMSOL simulations. This approach encompasses three main advantages: it is cheaper, it requires less labor force and gives access to a large number of physical quantities (velocity at any point, concentration at any point) which is not possible with the experimental model.

The first subsection concerns the validation of the sigmoidal model used for the initial $C_0(x)$ profile as well as its Fourier series. Second, the validation of the concentration map model, i.e. equation (16) is discussed. Finally, the procedure for extracting the sigmoid parameters from a given concentration profile is also assessed. All the tests have been performed with a single type of molecule with a concentration C_1 at the first inlet 1 and 0 at the second inlet. Several combinations of flow rates Q_1 and Q_2 have been tested, with flow rate values ranging from 0.5 nL· s −1 to 2.5 $\mathrm{nL \cdot s^{-1}}$. The concentration of the molecule at inlet 1 as well as its diffusion coefficient has also been tested but it turns out that they do not have any major impact on the shape of the curve.

3.1. Validation of the sigmoid model for the initial profile

First, COMSOL Multiphysics simulation of the Y-shaped junction described on Figure 1 is performed for different combinations of inlets flow rate and the cross-section concentration profile for $y = 0$ are exported. Then, the Curve Fitting toolbox of MATLAB with the Levenberg-Marquart algorithm is used to extract the optimal parameters of the sigmoid (d is assumed to be 0). Extracted parameters are then compared to the expected one. Figure 2 shows the results for $Q_1 = Q_2 = 0.5\ \text{nL} \cdot \text{s}^{-1}$ and $C_1 = 1\ \text{mM}$. The fitting of the concentration profile by the sigmoidal function is very good. The RMSE is less than 1% of the average concentration. The values of a and c are consistent with the expected ones: $a = C_1 = 1\ \text{mM}$ and $c = 5\ \mu\text{m}$ for a 10-µm width as $Q_1 = Q_2$.

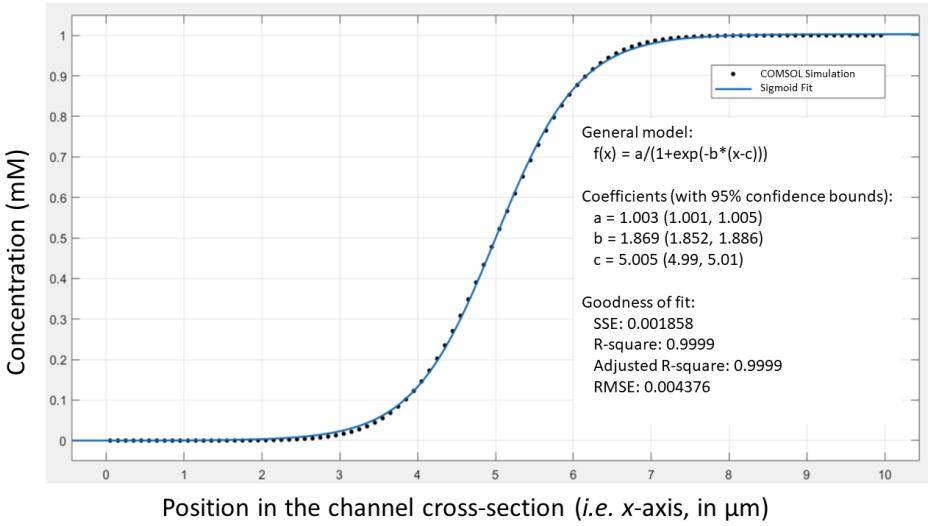

Figure 2. Fitting of the cross-section concentration profile at the input of the mixer with a sigmoidal function (MATLAB Curve Fitting Toolbox screenshot). The simulation results obtained with COMSOL (black dots) are fitted with a sigmoidal function given in equation (17) with $d = 0$ (blue curve). Simulations have been performed with $Q_1 = Q_2 = 0.5\ \text{nL} \cdot \text{s}^{-1}$ and $C_1 = 1\ \text{mM}$.

We also extracted the value of b for 25 combination of inlet fluxes Q_1 and Q_2. The linear relationship between b and the total flux $Q_{tot} = Q_1 + Q_2$ is confirmed with a high degree of confidence (see Figure 3): the relative error between extracted values for b and their linear interpolation is less than 10% over all the combinations (the RMSE is about 3%). For the Y-shaped junction geometry considered in this study, the values of k_1 and k_2 are respectively $0.605 \cdot 10^{-6}\ \text{s} \cdot \mu\text{m}^4$ and $1.31\ \mu\text{m}^{-1}$.

The second validation step consists of assessing the impact of the Fourier series decomposition of the sigmoid. For that purpose, we compare on the RMSE between the COMSOL simulations and the Fourier decomposition of the sigmoid, on the one hand, and the RMSE between the sigmoid fit of COMSOL simulations and its Fourier decomposition, on the other hand. Figure 4 shows the results. The right table highlights that, beyond the fifth order, the error introduced by the Fourier decomposition is lower than the one introduced by the sigmoid fit. Thus, it can be pointed out that the impact of using a Fourier series is negligible and only a few number of terms are required to obtain a good approximation of the sigmoidal function.

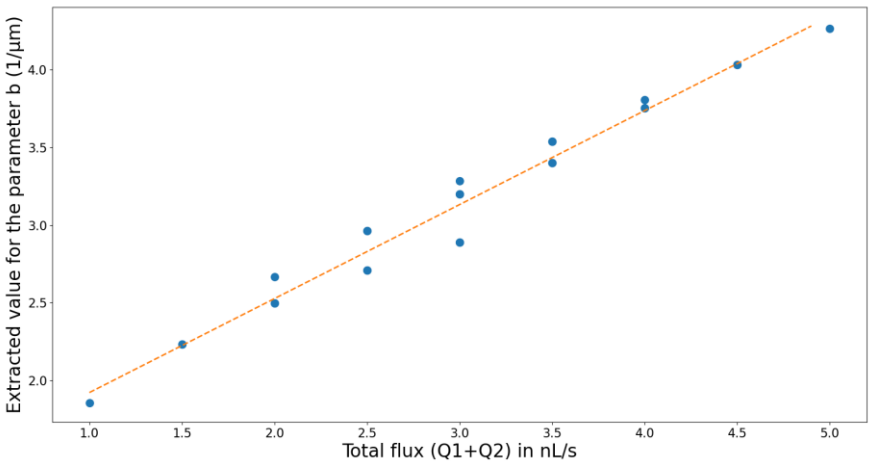

Figure 3. Linear interpolation of the extracted value of b and the total flux for 25 combinations of Q_1 and Q_2.

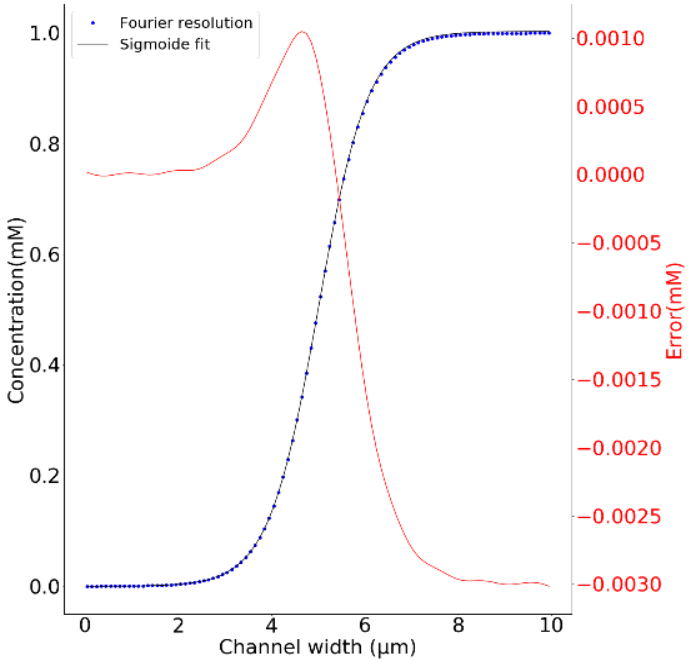

Fourier series order	Relative Error COMSOL vs Fourier	Relative Error Sigmoid vs Fourier
1	2.76 %	2.70 %
3	0.418 %	0.835 %
5	0.330 %	0.303 %
7	0.317 %	0.116 %
9	0.311 %	< 0.050 %

Figure 4. Impact of the Fourier series decomposition. The left plot compares the sigmoid equation (black curve) and its Fourier series decomposition (blue dots) in the same conditions as for Figure 2. The red curve gives the error introduced by the Fourier decomposition as a function of the position in the *x*-axis. The table on the right compares the relative error observed between COMSOL, the sigmoid fit and the Fourier series decomposition as a function of the order.

3.2. Validation of the model on the whole channel

In this subsection, the validity of the model of the concentration map inside the whole channel,

i.e. equation (17), is assessed. For that purpose, we compare again the map simulated with COMSOL and the map calculated with the analytical model. Figure 5A shows the difference between both maps for six different inlet flow rate combinations. It can be observed that the highest difference between the two models occurs rather at the beginning of the channel, where the two flows meet. At this point, velocity fields in the transverse direction might exist. They are natively taken into account by the COMSOL simulation but not in our model. This error can reach up to 10% percent but fades quickly along the channel. At the end of the channel, the RMSE decreases down to 1% (see Figure 5B). Figures 5C and 5D represent respectively the maximum error (in %) observed in the channel and at the end of the channel for 25 couples of input flows. According to these results, it can be pointed out that errors introduced by our model are acceptable.

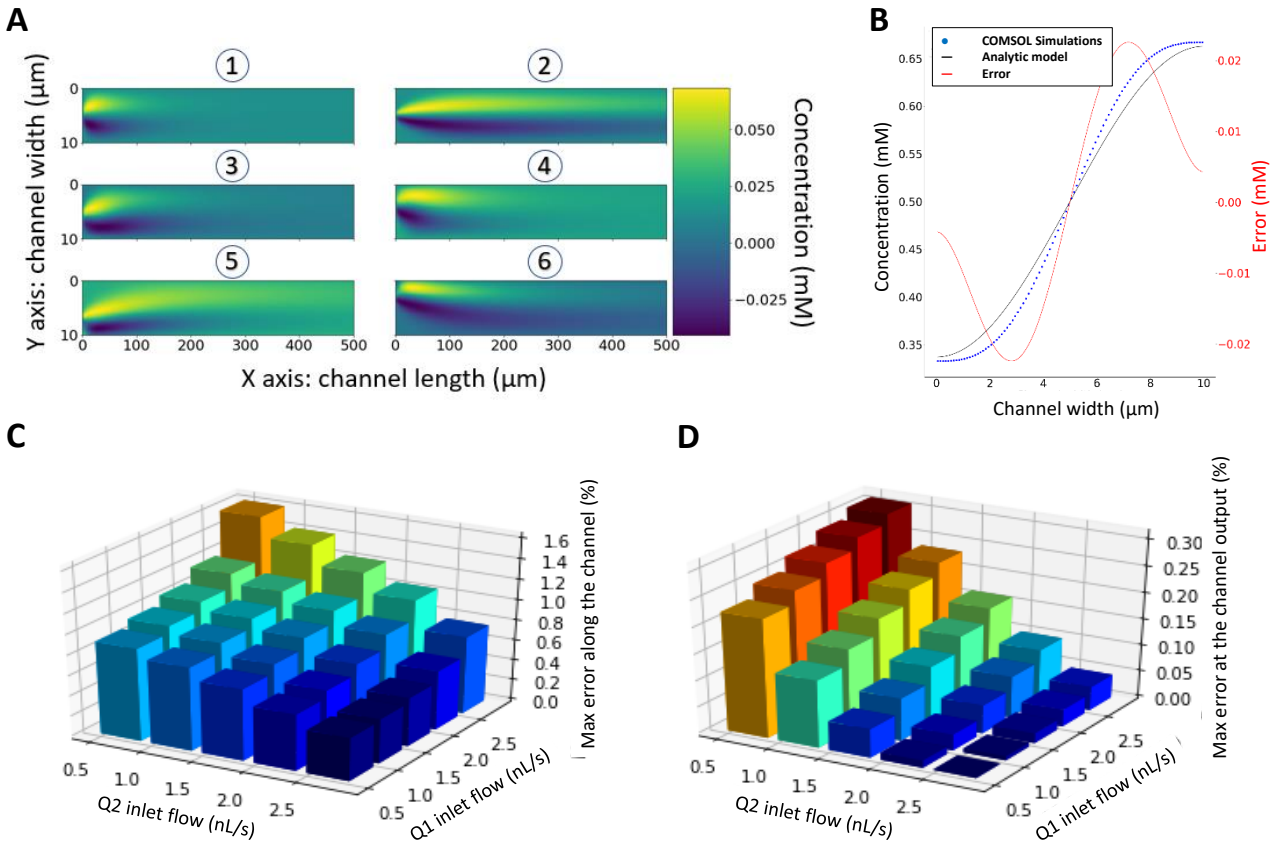

Figure 5. Simulation results for the validation of the model inside the channel. (A) is the error between COMSOL simulation and the analytic model for six different inlet flow rate combinations: Q_1 values are respectively 0.5, 2.5, 1, 0.5, 2.5 and 0.5 while Q_2 values are respectively 0.5, 2.5, 0.5, 1, 0.5 and 2.5. (B) gives the COMSOL simulation results, the result obtained with the analytical model and the error between both for $Q_1 = Q_2 = 1\ \mathrm{nL} \cdot \mathrm{s}^{-1}$. (C) gives the maximal error (in %) measured all along the channel for 25 different inlet flow rate combination. (D) gives the same data at the end of the channel.

3.3. Validation of the extraction procedure for the sigmoid parameters

The last validation step concerns the parameter extraction procedure for the sigmoidal function. For that purpose, we first calculate 1000 sigmoid functions $s_i(x)$ according to equation (18) for x in the range $[0; 10]\mu m$ with four parameters a, b, c and d randomly drawn in a range that suits with our application: $[0.1; 10]$ mM for a, $[0.5; 5]$ μm^{-1} for b, $[1; 9]$ μm for c and $[0; 1]$ mM for d. Then, we use the parameter extraction procedure to retrieve a, b, c and d from $s_i(x)$ and calculate the mean error (ME) and the RMSE between the original and the extracted values, as well as the RMSE between the original curve and the one obtained with the extracted parameters.

Parameters a and c are always very well estimated, without offset and with an RMSE of 240 ppm for a and 86 ppm for c. Parameters b and d are slightly underestimated with an ME of -0.5% for b and -0.3% for d. The RMSE is about 2% for b and 1.3% for d. Finally, the average RMSE between the original curve and the one obtained with extracted parameters is about 0.15%. These results validate our parameter extraction procedure.

4. Discussion

The analytical model presented in this paper is able to accurately predict the concentration profiles at the outlet of a passive mixer whatever its length. Compared with COMSOL simulations, which is our reference in the paper, the analytical model is more versatile and lighter in terms of computation resources. The model relies on two main assumtions: i) the laminar flow and ii) the sigmoid shape of the concentration profile at any point of the channel. It relies only on technological or physical parameters, except for two parameters (k_1 and k_2) which depends on the shape of the junction. Thus, the model might be adapted for a different junction shape after a required calibration step consisting of the extraction of k_1 and k_2 for the studied junction shape from experiments or finite element simulation. In a future work, it might be interesting to look for an empirical relationship between the junction geometry (angle, width of the channels, etc.) and k_1 and k_2.

The simplicity of the model enables its implementation with various types of computational languages. This includes, among others, Verilog-AMS, a hardware description language (HDL) used for the description and the design of electronics circuits and systems [27]. Verilog-AMS models of microfluidic devices under the assumption of homogeneous fluids have already been established [28,29]. At the same time, we also demonstrated the possibility to implement biochemical reaction models with such language [30], as well as reaction-advection-diffusion processes in microfluidic cavities [31]. The implementation of models for the passive mixers and other microfluidic devices exhibiting concentration gradients will thus enrich the library of building blocks with the ultimate focus on the *in silico* prototyping of lab-on-chip with a single language and environment [31].

Verilog-AMS models are composed of black boxes with two kinds of connections between each other: the nodes or terminals which corresponds to quantities linked together by the generalized Kirchhoff laws (current/voltage in electronics, pressure/flow in microfluidics) [27] on the one hand, and the free quantities used for signal-flow descriptions. The analytical model described in this paper might be used for the Verilog-AMS description of several microfluidics circuits (Figure 6):

- A short Y-shaped junction, which would be composed of three terminals (one for each inlet and one for the outlet), two input quantities (the concentration of the molecule of interest at each inlet) and four output quantities (the parameters of the sigmoid giving the concentration

profile at the output).

- A short non-uniform channel, which would be composed of two terminals (one for the inlet and one for the outlet), four input quantities and four output quantities (the parameters of the sigmoid giving the concentration profile at the input and at the output).
- A long non-uniform channel, which would be composed of two terminals (one for the inlet and one for the outlet), four input quantities (the parameters of the sigmoid giving the concentration profile at the input) and one single output quantity (the concentration which is assumed to be homogeneous after a long channel).
- A Y-shaped splitter with long channels, which would be composed of three terminals (one for the inlet and one for each outlet), four input quantities (the parameters of the sigmoid giving the concentration profile at the input and at the output) and two output quantities (the concentration which is assumed to be homogeneous on each branch of the Y-shaped splitter).

For all of these models, between pressure and flow rate are linked together according to the microfluidic/electronic analogies and generalised Kirchhoff laws. Besides, the relationship between free quantities is computed with the analytic models and integral calculation of the concentration across the channel width. All of these models might be combined together to obtain a complex microfluidic network. An example of model composition is given in [32]: we showed that the analytic model computed the same concentration map for a Y-shaped junction with a 500µm-long channel and for a Y-shaped junction with a 250µm-long channel followed by a 250µm-long short channel.

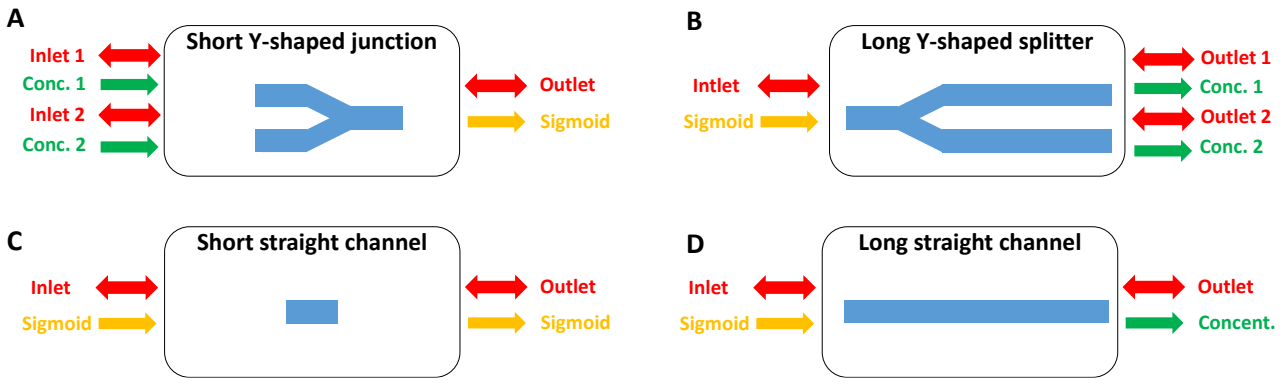

Figure 6. Examples of Verilog-AMS compact models of microfluidic devices based on our analytical model. (A) is a short Y-shaped junction described in detail this paper. (B) is a splitter for which the input has a sigmoid concentration profile. Output channels are long enough to meet in the homogeneous fluid assumption at the output. The concentration inside each branch of the splitter is computed by integration of the concentration profile just before the splitter. (C) is the short straight channel with sigmoid concentration profile at the input and the output. (D) is a channel long enough to meet in the homogeneous fluid assumption at the output. The concentration at the output is the integral of the concentration profile over the whole channel section.

Up to that point, we only discussed microfluidic devices with a single molecule of interest. However, most of the microfluidic mixers involve two or more chemical compounds. The complete model for a microfluidic system with multiple molecules of interest is a set of PDEs composed of one

instance of equation (2) per molecule. If no reaction occurs, i.e. $s(t,x,y)=0$, each equation is independent and can be solved separately. Thus, the resulting analytical model is simply a superposition of analytical models, one per molecule. Additional free quantities are added to the model, one per molecule (corresponding to its concentration) when fluid are considered to be homogeneous and four per molecule (the parameters of the sigmoid) otherwise.

The problem is much more complex when reactions occur in the channel. In this case, equations are no more independent and the coupling makes its analytical resolution very tricky. However, two extreme situations deserve to be discussed. If the reaction rate in low compared to the time it takes for the molecule to cross the channel from end to end, $s(t,x,y)$ can be neglected and only the reactants have to be considered. Conversely, if the reaction rate is high enough, we can consider that biochemical process is always at its steady state. Thus we first calculate the map of the reactant with the analytical model and then calculate the biochemical equilibrium state with the biochemical reactions. In between, the only way to take reaction into account is to solve numerically the set of couples PDEs with finite element methods. COMSOL provides specific modules for that purpose.

The last point that deserves to be discussed is the assumption of the sigmoid profile of the concentration, which is the most common profile encountered in the case of a two-fluid mixture. However, other profiles might be observed, for instance if one considers a three-inlet mixer. In such cases, more complex, deserve deeper investigation. In such cases, several avenues can already be put forward. One of them consists of adapting the profile function and, thus, changing the set of parameters that characterize the profile. Equation (15) suggests that the concentration profile is conserved along the channel. Thus, as soon as we have a mathematical equation for the profile at the input of the channel, the associated Fourier coefficients can be calculated and altered by equation (15), and then used to compute the output concentration profile. Another alternative would be to keep sigmoid function but to characterize an actual profile as a superposition of sigmoidal functions. In this case, the structure of the model is not affected: superposition of sigmoidal functions can be treated just as in the case of multiple molecules problems. This is a kind of equivalent in microfluidic of the superposition theorem in electronics. Of course, this approach has to be verified and assessed on a large range of circuits, but we already demonstrate its validity in the case of a circuit mixing the same molecule at different concentration and at different flow rate. The concentration map inside the channel is always equal to the sum of the concentration map considering that there are only molecules at the first inlet and the map considering that there are only molecules at the second inlet. In particular, if the concentration of both inlets are equal, whatever the flow rate, the resulting concentration map is homogeneous, which is in accordance with the theoretical expectations.

5. Conclusions

The paper describes an analytical model for passive mixers by departing from the assumption of a channel long enough to ensure a homogeneous mixing. The model relies on a few analytical equations, some numerical integrations to compute the Fourier coefficients and an iterative curve fitting procedure. It is therefore quite light from a computational point of view compared to a finite element model. This approach gives very satisfactory results in the case of a simple Y-shaped mixer but might also be used to describe more complex behaviors (mixing of several molecules, multi-input mixer). One of the strengths this modelling approach is interoperable together with other models of microfluidic devices, but also biochemical and electronic devices, in a modelling environment based

on hardware description languages (Verilog-AMS for instance). It is thus a step forward towards a plug-and-play *in silico* prototyping environment for lab-on-a-chip.

Acknowledgments

This research was supported by the European Regional Development Fund (ERDF) and the Interreg V Upper Rhine Offensive Sciences Program (Project 3.14 – Water Pollution Sensor).

Conflict of interest

The authors declare no potential conflicts of interest

References

1. P. Cui, S. Wang, Application of microfluidic chip technology in pharmaceutical analysis: A review, *J. Pharmaceut. Ana.,* **9** (2019), 238–247. https://doi.org/10.1016/j.jpha.2018.12.001
2. M. Tokeshi, Applications of microfluidic systems in biology and medicine, Springer, (2019). https://doi-org/10.1007/978-981-13-6229-3
3. S. Li, Z. Ma, Z. Cao, L. Pan, Y. Shi, Advanced wearable microfluidic sensors for healthcare monitoring, *Small,* **16** (2020), 1903822. https://doi.org/10.1002/smll.201903822
4. M. Yew, Y. Ren, K. S. Koh, C. Sun, C. Snape, A review of state-of-the-art microfluidic technologies for environmental applications: Detection and remediation, *Global Challenges,* **3** (2019), 1800060. https://doi.org/10.1002/gch2.201800060
5. U. Hashim, P. N. A. Diyana, T. Adam, Numerical simulation of Microfluidic devices, *2012 10th IEEE International Conference on Semiconductor Electronics (ICSE)*, (2012), 26–29. https://doi.org/10.1109/SMElec.2012.6417083
6. D. Erickson, Towards numerical prototyping of labs-on-chip: Modeling for integrated microfluidic devices, *Microfluid Nanofluid,* **1** (2005), 301–318. https://doi-org/10.1007/s10404-005-0041-z
7. P. Hadikhani, S. Majidi, A. Afshari, Numerical simulation of droplet formation in different microfluidic devices, *P. I. Mech. Eng. C-J Mec.,* **234** (2020), 3776–3788. https://doi.org/10.1177/0954406220916480
8. J. Wang, V. G. J. Rodgers, P. Brisk, W. H. Grover, Instantaneous simulation of fluids and particles in complex microfluidic devices. *PLOS ONE,* **12** (2017), e0189429. https://doi.org/10.1371/journal.pone.0189429
9. R. Qiao, N. R. Aluru, A compact model for electroosmotic flows in microfluidic devices, *J. Micromec.h Microeng.,* **12** (2002), 625–635.
10. W. Jeon, C. B. Shin, Design and simulation of passive mixing in microfluidic systems with geometric variations, *CAN. J. Chem. Eng.,* 152 (2009), 575–582. https://doi.org/10.1016/j.cej.2009.05.035
11. A. Maha, D. O. Barrett, D. E. Nikitopoulos, S. A. Soper, M. C. Murphy, Simulation and design of micromixers for microfluidic devices, *P. SoC Photo-Opt. Ins.*, International Society for Optics and Photonics, (2003),183–193. https://doi.org/10.1117/12.530788
12. J. Koo, C. Kleinstreuer, Liquid flow in microchannels: Experimental observations and computational analyses of microfluidics effects, *J. Micromech. Microeng.,* **13** (2003), 568–579. https://doi.org/10.1088/0960-1317/13/5/307

13. C. Y. Lee, W. T. Wang, C. C. Liu, L. M. Fu, Passive mixers in microfluidic systems: A review, *CAN. J. Chem. Eng.,* **288** (2016), 146–160. https://doi.org/10.1016/j.cej.2015.10.122
14. Y. K. Suh, S. Kang, A Review on Mixing in Microfluidics, *Micromachines,* **1** (2010), 82–111. https://doi.org/10.3390/mi1030082
15. P. Tabeling, Introduction to Microfluidics, Oxford University Press, USA, 2005.
16. W. Hundsdorfer, J. Verwer, Numerical Solution of Time-Dependent Advection-Diffusion-Reaction Equations, Springer-Verlag Berlin Heidelberg, 2003.
17. I. M. Hsing, R. Srinivasan, M. P. Harold, K. F. Jensen, M. A. Schmidt, Finite element simulation strategies for microfluidic devices with chemical reactions, *Proceedings of International Solid State Sensors and Actuators Conference (Transducers '97)*, **2** (1997), 1015–1018. https://doi.org/10.1109/SENSOR.1997.635357
18. Comsol, COMSOL Multiphysics® Modeling Software, 2019.
19. Microfluidics Software—For Simulating Microfluidics Devices. Available from: https://www.comsol.fr/microfluidics-module
20. C. Prud'homme, V. Chabannes, V. Doyeux, M. Ismail, A. Samake, G. Pena, Feel++: A computational framework for Galerkin Methods and Advanced Numerical Methods, *ESAIM Proceed.,* **38** (2012), 429–455. https://doi.org/10.1051/proc/201238024
21. N. Zaidon, A. N. Nordin, A. F. Ismail, Modelling of microfluidics network using electric circuits, *2015 IEEE Regional Symposium on Micro and Nanoelectronics (RSM)*, (2015), 1–4. https://doi.org/10.1109/RSM.2015.7354954
22. K. W. Oh, K. Lee, B. Ahn, E. P. Furlani, Design of pressure-driven microfluidic networks using electric circuit analogy, *Lab Chip,* **12** (2012), 515–545. https://doi.org/10.1039/C2LC20799K
23. M. H. V. Werts, V. Raimbault, R. Texier-Picard, R. Poizat, O. Français, L. Griscomab, et al., Quantitative full-colour transmitted light microscopy and dyes for concentration mapping and measurement of diffusion coefficients in microfluidic architectures, *Lab Chip,* **12** (2012), 808–820. https://doi.org/10.1039/c2lc20889j
24. F. A. Perdigones, A. Luque, J. M. Quero, Correspondence between electronics and fluids in mems: designing microfluidic systems using electronics, *IEEE Indust. Electron. Magaz.,* **8** (2014), 6–17. https://doi.org/10.1109/MIE.2014.2318062
25. H. Xie, X. Zhao, H. Yang, Experimental and numerical study on a planar passive micromixer with semicircle mixing elements, *2010 IEEE/ASME International Conference on Advanced Intelligent Mechatronics*, (2010), 1013–1016. https://doi.org/10.1109/AIM.2010.5695817
26. H. L. The, H. L. Thanh, T. Dong, Q. B. Ta, N. Tran-Minh, F. Karlsen, An effective passive micromixer with shifted trapezoidal blades using wide Reynolds number range, *Chem. Eng. Res. Des.,* **93** (2015), 1–11. https://doi.org/10.1016/j.cherd.2014.12.003
27. K. Kundert, O. Zinke, The Designer's Guide to Verilog-AMS, Springer US, 2004. https://doi.org/10.1109/BMAS.2009.5338896
28. Y. Zeng, F. Azizi, C. H. Mastrangelo, Behavioral modeling of solute tracking in microfluidics, *2009 IEEE Behavioral Modeling and Simulation Workshop*, (2009), 1–6. https://doi.org/10.1109/BMAS.2009.5338896
29. A. Voig, J. Schreiter, P. Frank, C. Pini, C. Mayr, A. Richter, Method for the computer-aided schematic design and simulation of hydrogel-based microfluidic systems, *IEEE T Comput. Aid. D.* **39** (2010), 1635–1648. https://doi.org/10.1109/TCAD.2019.2925354
30. Y. Gendrault, M. Madec, C. Lallemen, J. Haiech, Modeling biology with HDL languages: A first

step toward a genetic design automation tool inspired from microelectronics, *IEEE T Bio-med. Eng.* **61** (2014), 1231–1240. https://doi.org/10.1109/TBME.2014.2298559

31. M. Madec, L. Hebrard, J. B. Kammerer, A. Bonament, E. Rosati, C. Lallement, Multiphysics simulation of biosensors involving 3d biological reaction-diffusion phenomena in a standard circuit EDA environment, *IEEE T. Circuits-I Regular Papers,* (2019), 1–10. https://doi.org/10.1109/TCSI.2018.2885223
32. A. Bonament, A. Prel, J. M. Sallese, M. Madec, C. Lallement, Compact model for continuous microfluidic mixer, *2020 27th International Conference on Mixed Design of Integrated Circuits and System (MIXDES)*, (2020), 35–39. https://doi.org/10.23919/MIXDES49814.2020.9155997

AIMS Press

©2022 the Author(s), licensee AIMS Press. This is an open access article distributed under the terms of the Creative Commons Attribution License (http://creativecommons.org/licenses/by/4.0)